Inorganic Chemistry

Article

pubs.acs.org/IC

Neutron Diffraction Studies of the Molecular Compound $[Co_2(bta)]_n$ (H_4bta =1,2,4,5-Benzenetetracarboxylic Acid): In the Quest of Canted Ferromagnetism

Oscar Fabelo,*[,†,‡] Laura Cañadillas-Delgado,[†,⊥] Jorge Pasán,*[,§] Pau Díaz-Gallifa,[§] Catalina Ruiz-Pérez,[§] Francesc Lloret,[∥] Miguel Julve,[∥] Inés Puente Orench,[†,‡] Javier Campo,[†] and Juan Rodríguez-Carvajal[‡]

[†]Instituto de Ciencia de Materiales de Aragón, CSIC-Universidad de Zaragoza, C/Pedro Cerbuna 12, E-50009 Zaragoza, Spain

[‡]Institut Laue-Langevin, Grenoble, 6 rue Jules Horowitz, BP 156, 38042 Grenoble Cedex 9, France

[§]Laboratorio de Rayos X y Materiales Moleculares, Departamento de Física Fundamental II, Universidad de La Laguna, Tenerife, Avda. Astrofísico Francisco Sánchez s/n, E-38204 La Laguna, Tenerife, Spain

[∥]Instituto de Ciencia Molecular/Departament de Química Inorgànica, Universitat de València, C/Catedrático José Beltrán 2, 46980 Paterna (València), Spain

[⊥]Centro Universitario de la Defensa de Zaragoza, Ctra de Huesca s/n, 50090 Zaragoza, Spain

Supporting Information

ABSTRACT: The exchange mechanism and magnetic structure of the organic−inorganic layered molecule-based magnet $[Co_2(bta)]_n$ (**1**) (H_4bta =1,2,4,5-benzenetetracarboxylic acid) have been investigated through variable-temperature magnetic susceptibility measurements and supported with a series of neutron diffraction experiments. Cryomagnetic studies have shown an antiferromagnetic ordering at a transition temperature of 16 K that is followed by the appearance of a weak ferromagnetism below 11 K. The weak antiferromagnetic interlayer interaction plays an important role in this system in spite of the long interlayer separation. A ferromagnetic ordering is induced by applied magnetic fields greater than 1800 G (metamagnetic behavior), and a slow magnetic relaxation from this ferromagnetic phase to the antiferromagnetic one is observed. The magnetic structure of **1** has been elucidated at low temperatures in zero field by neutron powder diffraction measurements and was found to be of antiferromagnetic nature with the local cobalt(II) spins (magnetic moments) being aligned ferromagnetically in the *ac* plane and antiferromagnetically coupled along the crystallographic *b* axis. No evidence for a long-range spontaneous ferromagnetic component below 11 K was observed in the neutron experiment.

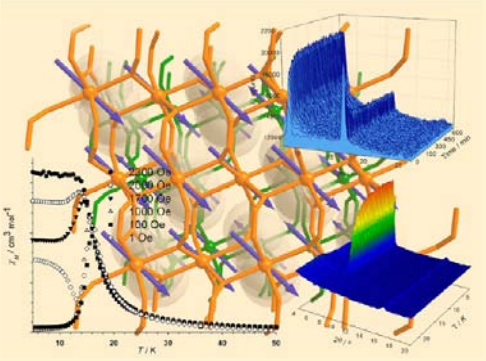

INTRODUCTION

One of the areas of solid-state chemistry that has shown remarkable growth over the last two decades is the synthesis and characterization of organic and metal−organic magnetic materials.[1] As part of our ongoing research on low-dimensional molecule-based materials, we focus here on the correlations between the crystal structure and magnetic properties.[2] The presence of anisotropy, crystal and/or dipolar field, and/or antisymmetric exchange can perturb layered systems and introduce some 3D character, which finally results in 3D long-range ordering at finite temperatures.[3] The orientation of the moments of the magnetic atoms and their consequences on the magnetic properties are of particular interest. To determine the magnetic structure present in the bulk, the most direct method is neutron diffraction.[4] Nevertheless, neutron studies of metal−organic compounds are not really common among the inorganic chemistry community[5] because one of the most important drawbacks arises from the strong incoherent scattering of the hydrogen nucleus as well as the difficulties of organic moiety deuteration, which is unfortunately not always accessible.

The crystal structure of the 3D $[Co_2(bta)]_n$ (1) [H_4bta = 1,2,4,5-benzenetetracarboxylic acid (commonly known as pyromellitic acid)] compound was solved by single-crystal X-ray diffraction some years ago, but its magnetic behavior has been the subject of controversy. Basically, two different models have been proposed on the basis of the magneto-structural studies. The first one reported by Snejko et al. states, "For low fields (H < 2 kOe < H_c), the magnetic susceptibility shows a clear cusp at 14.9 K that could be interpreted as antiferromagnetic ordering or a reduction in susceptibility due to the formation of randomly oriented ferromagnetic domains. For higher fields, the susceptibility is clearly saturated at temperatures below T_C, as expected for a ferromagnet". The second report was presented by Kumagai et al.[6b] and states,

Received: August 27, 2013
Published: October 16, 2013

Table 1. Final Atomic Coordinates, Isotropic Temperature Factors, and Fractional Occupancies Atomic Parameter of 1 Obtained through High-Resolution Neutron Diffraction at 20 K

atom	site[a]	*x*/*a*	*y*/*b*	*z*/*c*	B_{iso} (Å^2)	occ.[b]
Co(1)	4h	0.00000	0.2091(5)	0.50000	0.94(16)	0.5
O(1)	8j	0.2417(4)	0.29981(16)	0.7125(5)	0.54(5)	1.0
O(2)	8j	0.2930(4)	0.36619(15)	1.1578(6)	0.50(5)	1.0
C(1)	8j	0.2109(4)	0.35961(13)	0.8523(5)	0.37(4)	1.0
C(2)	8j	0.0911(3)	0.42987(14)	0.6615(5)	0.40(4)	1.0
C(3)	4i	0.1763(5)	0.50000	0.8186(7)	0.41(6)	0.5
H(1)	4i	0.3158(10)	0.50000	1.0636(16)	2.17(12)	0.5

[a]Space group = *C*2/*m* (No. 12). [b]Occupation is given as the multiplicity of the site divided by multiplicity of the space group.

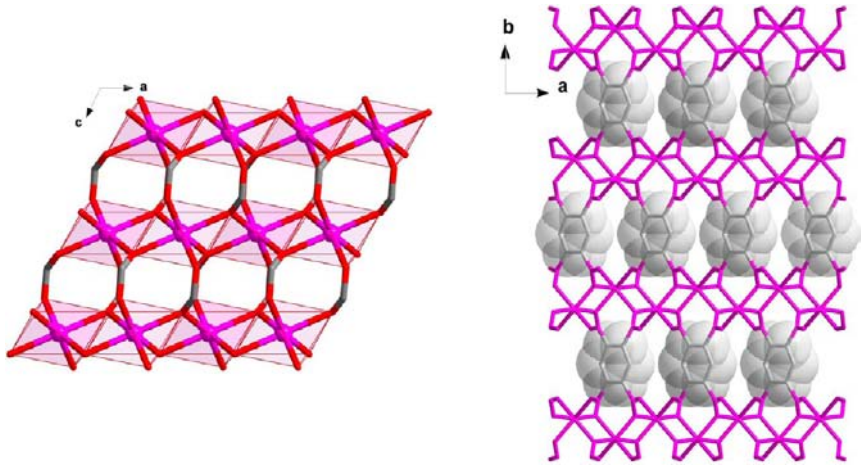

Figure 1. (a) View of a fragment of **1** along the crystallographic *b* axis showing the double μ-oxo(carboxylate) bridged cobalt(II) chains running parallel to the *a* axis and their interconnection across the *anti-syn* carboxylate bridges. (b) View of the 3D crystal structure of **1** along the crystallographic *c* axis showing the connections between the layers of cobalt(II) ions.

"Compound **1** exhibits a very unusual magnetic behavior, with three ground states (collinear and canted antiferromagnetism and field-induced ferromagnetism).... To account for the collinear antiferromagnetic ordering at 16 K, two scenarios can be envisaged. One is that the arrangement of the moments is antiparallel ferromagnetic chains and the second is antiparallel ferromagnetic layers.... The origin of the canting in these compounds is still a mystery.... In the absence of a neutron diffraction study we can only speculate on the magnetic structure of **1**...." Most of the irreversibility and irreproducibility of the magnetic properties observed by different authors could not be explained.[6] However, they can be easily understood because of the occurrence of a slow magnetic relaxation from the field-induced ferromagnetic phase toward the antiferromagnetic state, as shown in the present article. In view of the diversity of the magnetic phenomena generated in this 3D framework, we have decided to study this compound to shed light onto its magnetic behavior.

In this contribution, we present a study of the correlation between the crystal and magnetic structures of **1** based on variable-temperature macroscopic magnetic measurements (SQUID) and neutron powder diffraction experiments in the presence and absence of an external applied field. These experiments clearly provide the identification of the magnetic scattering and its temperature dependence, leading to the determination of the long-range-ordered magnetic structure.

EXPERIMENTAL SECTION

Materials. Single crystals and powder samples of **1** were prepared following an adaptation of the procedure described in the literature because neither of the syntheses previously described yielded a product without impurities.[6] Reagents and solvents used in the synthesis were purchased from commercial sources and used without further purification. The tetracarboxylic H_4bta derivative was used without deuteration. Elemental analyses (C, H, and N) were performed with an EA 1108 CHNS/0 automatic analyzer.

Physical Measurements. Magnetic susceptibility measurements on polycrystalline samples of **1** were carried out in the temperature range 1.9−300 K with a Quantum Design SQUID magnetometer. Corrections for the diamagnetic contribution of the constituent atoms and for the magnetization of the sample holder were applied.

Crystal Structure Determination and Refinement. Neutron powder diffraction experiments were performed on the high-resolution multidetector and on the high-intensity powder diffractometers D1A and D1B, respectively, at the Institut Laue−Langevin in Grenoble (France). The sample was contained in a 6 mm cylindrical vanadium can and placed on a cryostat (vanadium-tailed Cryostat 69ILHV25 and Joule Thomson Cryostat 148ILJT49 for D1B and D1A, respectively) and on a TASMAG Cryomagnet 96OXHV50 for measurements under an external magnetic field, which were collected at the D1B diffractometer. For measurements under an applied magnetic field, the sample was mixed with deuterated 2-propanol-d_8 and quenched to 70 K to avoid the crystallization of the 2-propanol-d_8. Once the 2-propanol-d_8 is in an amorphous solid state, the orientation of the powder sample will be constant independently on the external applied field. The data sets were collected with calibrated neutrons of wavelengths 2.5250 and 1.9076 Å for D1B and D1A, respectively. The diffraction patterns were recorded in the temperature range from 2.0 to 20 K with and without an applied magnetic field (up to 2 T) at D1B. A further high-resolution neutron diffraction profile was collected at 20 K in the D1A diffractometer. The crystal structure was refined by the Rietveld method using the FullProf suite of programs[7] from an initial model derived from single-crystal X-ray

dx.doi.org/10.1021/ic402186p | *Inorg. Chem.* 2013, 52, 12818−12827

diffraction data collected on a Nonius Kappa CCD diffractometer at 100 K (Tables 1 and S1 in the Supporting Information).

Synthesis of $[Co_2(bta)]_n$ (1). 1,2,4,5-Benzenetetracarboxylic acid anhydride (pyromellitic anhydride) (0.22 g, 1 mmol) was dissolved in water (15 cm^3) containing tetrabutylammonium hydroxide (0.36 g, 4 mmol). Cobalt(II) nitrate hexahydrate (0.59 g, 2 mmol) dissolved in water (3 cm^3) was then added to the previous aqueous solution. The pink slurry obtained was placed in a 23 mL Teflon-lined stainless steel reactor, which was then heated at 175 °C for 120 h. The reactor was cooled to room temperature, affording violet crystals. Three separate batches were combined to generate 1.7 g of crystals of $[Co_2(bta)]_n$. The purity of the product was confirmed through X-ray and high-resolution neutron powder diffraction. Anal. Calcd for $C_{10}H_2Co_2O_8$ (**1**): C, 32.64; H, 0.55. Found: C, 32.60; H, 0.48.

RESULTS AND DISCUSSION

Description of the Crystal Structure of 1. The X-ray structure of **1** consists of organic−inorganic layers of cobalt(II) ions that grow in the *ac* pane and that are linked through the pyromellitate skeleton to form a 3D network. Within each layer, uniform zigzag chains of double oxo(carboxylate)-bridged cobalt(II) ions running along the crystallographic *a* axis are connected through *anti-syn* carboxylate-bridges along the *c* direction (Figure 1a). Therefore, each cobalt(II) ion is linked to six neighbors within each layer, with two of them along the *a* axis (the shortest intrachain cobalt−cobalt separation is 3.368 Å) and the other four belonging to the adjacent chains (metal−metal separation through the *anti-syn* carboxylate bridges ranging from 4.475 to 4.554 Å). The topological analysis shows that the inorganic layers are built of 6-fold nodes, giving rise to the $[4^66^65^3]$-**hex** net in Schläfli notation.[8] The benzene rings of the pyromellitate ligand connect the layers into a 3D framework through the seven-atom pathway Co−O−C−C−C−C−C−O−Co, with a metal−metal separation of 8.788 Å (Figure 1b). Each Co(II) ion is in an elongated octahedral environment with Co−O bond lengths spanning the range of 2.034(4)−2.190(8) Å (Table 2). The pyromellitate ligand in **1** is fully deprotonated. As is shown in previous works, the versatility of the pyromellitate ligand in its cobalt(II) complexes accounts for the variety of its coordination modes,[9] being attached to 10 cobalt(II) ions in **1** through 12 coordination bonds.

Table 2. Selected Bond Lengths (Angstroms) and Angles (Degrees) for 1[a,b]

	20 K	100 K
Co(1)−O(1)	2.039(8)	2.078(2)
Co(1)−O(1)$^{a-1}$	2.190(8)	2.195(3)
Co(1)−O(2)$^{b-1}$	2.034(4)	2.028(2)
O(2)$^{b-1}$ −Co(1)−O(2)$^{c-1}$	97.27(13)	97.67(8)
O(2)$^{b-1}$−Co(1)−O(1)	159.63(13)	159.00(8)
O(2)$^{b-1}$−Co(1)−O(1)$^{d-1}$	92.53(13)	93.40(8)
O(2)$^{b-1}$−Co(1)−O(1)$^{a-1}$	87.23(14)	87.33(9)
O(2)$^{b-1}$−Co(1)−O(1)$^{e-1}$	86.19 (13)	86.48 (9)
O(1)−Co(1)−O(1)$^{d-1}$	84.07(14)	82.07(8)
O(1)−Co(1)−O(1)$^{a-1}$	111.30(13)	111.20(9)
O(1)−Co(1)−O(1)$^{e-1}$	76.46(14)	76.24(9)
O(1)$^{a-1}$−Co(1)−O(1)$^{e-1}$	170.04(14)	170.59(9)

[a]Data at 20 K were obtained from neutron powder diffraction refinements (D1A, ILL), whereas those at 100 K were obtained using single-crystal X-ray diffraction (see the Supporting Information). [b]Symmetry codes: $(a-1) = -0.5+x, 0.5-y, z$; $(b-1) = -0.5+x, 0.5-y, -1+z$; $(c-1) = 0.5-x, 0.5-y, 2-z$; $(d-1) = -x, y, 1-z$; and $(e-1) = 0.5-x, 0.5-y, 1-z$.

Magnetic Properties of 1. Magnetic susceptibility measurements of **1** were recorded as a function of temperature upon cooling from room temperature until 1.8 K (Figure 2).

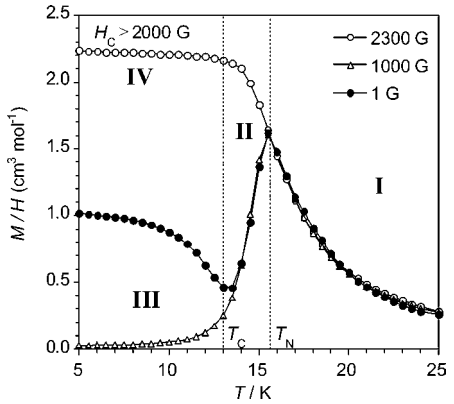

Figure 2. Magnetic susceptibility data for **1** at different external magnetic fields showing the four different magnetic regions: paramagnetism (I), collinear antiferromagnetism (II), canted antiferromagnetism (III), and field-induced ferromagnetism (IV).

The magnetic properties of **1** are quite complex, and the four different regions observed in this compound (paramagnetism (I), collinear antiferromagnetism (II), canted antiferromagnetism (III), and field-induced ferromagnetism (IV) in Figure 2) have been previously discussed.[6]

From rt to 20 K, the behavior is governed by ferromagnetic interactions between nearest-neighbor cobalt(II) ions. These ferromagnetic interactions are associated with the μ-oxo-(carboxylate) bridge along the *a* axis and the *anti-syn* carboxylato bridge along the *c* axis, forming the ferromagnetic *ac* plane.[10]

The maximum around 16 K is due to an antiferromagnetic ordering. The weak antiferromagnetic interaction could be mediated by the pyromellitate skeleton along the *b* axis.[11] Below the ordering temperature, χ_M rapidly decreases under small magnetic fields. When the magnetic field increases, the maximum of χ_M increases its intensity and shifts to lower temperatures. For $H > 2000$ G, it disappears, and the magnetization attains saturation (Figure 3a). This phenomenon corresponds to a metamagnetic behavior[12] (Figure 3b) that can be observed in the isothermal magnetization measurements (see below and Figure 4).

When very low fields are applied ($H = 1$ G), a sharp increase of magnetization is observed below 13 K. For $H > 100$ G, the magnetization becomes saturated without the observation of the above sharp increase. This abrupt increase was attributed to a spin canting with an extremely small canting angle (ca. 10^{-4} degrees).[13] The saturation of the magnetic moment of the spin canting under 1 G is very small [$M_{canting} \approx 1$ cm^3 mol^{-1} G $\approx 1.8 \times 10^{-4}$ BM compared to ca. 2.2 μ_B for the saturation value for a six-coordinate Co(II) ion].[10] The value of the saturation magnetization of the spin canting ($M_{canting}$) decreases gradually with the applied field (Figure 3b), suggesting that the moments of the sublattices rotate proportionally to the strength of the applied field. For $H > 1000$ G (inset of Figure 3b), the saturation value increases rapidly up to the expected value for a six-coordinate Co(II) ion.[14]

dx.doi.org/10.1021/ic402186p | Inorg. Chem. 2013, 52, 12818−12827

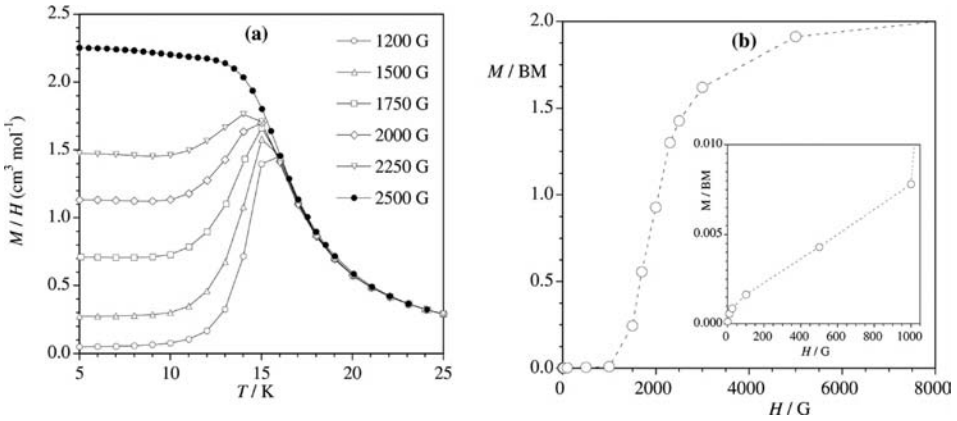

Figure 3. (a) Field-cooled magnetization data for **1** at different external magnetic fields. (b) Representation of the values of the saturation magnetization obtained from the field-cooled magnetization measurements under different applied magnetic fields as indicated in panel a. The inset shows the region of the low magnetic fields.

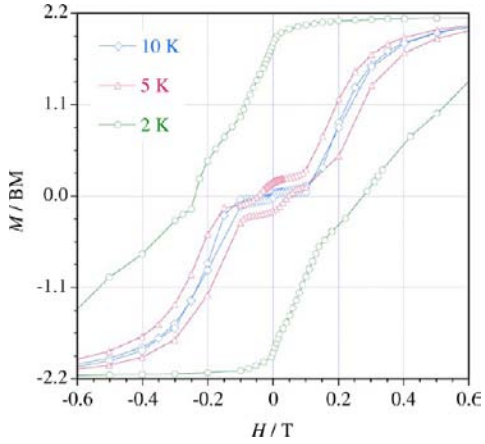

Figure 4. Detail of the hysteresis loops for a polycrystalline sample of **1** at three different temperatures (2, 5, and 10 K). The magnetic field is given in tesla.

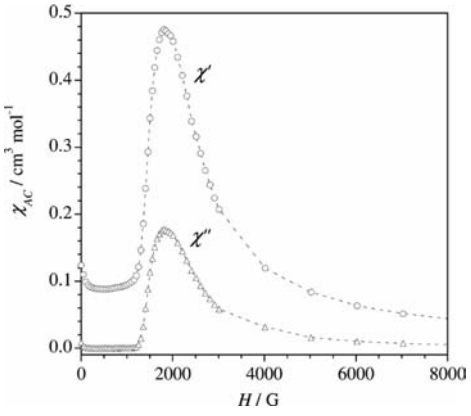

Figure 5. ac-magnetic susceptibility data for **1** as a function of applied magnetic field at 11 K and an oscillating frequency of 333 Hz. The upper and lower part depict the in-phase (χ') and out-of-phase (χ'') data, respectively.

The isothermal magnetization was measured at several temperatures (2−10 K) and field ranges and always followed the same protocol. The data were taken after a zero field cooled (ZFC) process and thereafter the first magnetization curves and the magnetization loops were measured (Figure 4). For $2 < T < 16$ K, all of these magnetization curves present a sigmoidal shape characteristic of a metamagnetic behavior with a critical field of about 1800 G, in agreement with the field cooled magnetization (FCM) measurements (Figure 3b). This field-induced ferromagnetic transition is also confirmed by field-dependent ac-susceptibility measurements. Figure 5 shows the real and imaginary components (χ' and χ'') of the ac-susceptibility, and both components present a maximum at $H \approx 1800$ G. Additionally, the occurrence of the weak ferromagnetism is confirmed by the ac-susceptibility measurements (Figure 6). The in-phase component of the susceptibility (χ') exhibits a maximum at 16 K (collinear AF ordering), whereas the out-of-phase component (χ'') shows one peak at 11 K (spin-canted ordering) together with a weak shoulder at 16 K.

For $T < 11$ K, the magnetization curves exhibit hysteresis loops with values of the coercive field (H_C) and remnant magnetization (M_R) increasing inversely with the temperature (i.e., H_C/M_R = 30 G/0.01μ_B (10 K) and 500 G/0.16μ_B (5 K)). No hysteresis was observed for $T > 11$ K. At $T \leq 2$ K, the magnetization curve does not present the sigmoidal shape, but presents a shape that is typical for a ferromagnet with a remnant magnetization $M_R = 2.0\mu_B$ (which is very close to the saturation value 2.2μ_B) and coercive field H_C = 2500 G (Figure 4). This curious feature is due to a slow magnetic relaxation of the ferromagnetic phase toward the antiferromagnetic state. That is, when the magnetic field decreases from 5 T to zero, a rapid decrease of the magnetization for fields near to the critical field, $H_{meta} \approx 1800$ G, would be expected (metamagnetic behavior). However, the magnetization decreases so slowly at 2 K that in the measuring time the compound behaves like a ferromagnet.[15]

To study this relaxation of the magnetization, time-dependent magnetization measurements at several temperatures were performed. For each temperature, the sample was cooled to 2 K at zero applied field from 40 K; then, a magnetic field of 2 T was applied to the sample during 10 min, and the data collection started just after its removal. The value of the magnetization measured under an external applied field of 2 T is 2.2μ_B, a value that remains constant for all of the measurements. Figure 7 shows the time-dependent magnetization at different temperatures. As one can see, the relaxation process is accelerated by the increase of the temperature, indicating the occurrence of thermally activated energy barriers.

It is interesting to note that the small frequency dependence observed in the out-of-phase ac-susceptibility (Figure 6) could

dx.doi.org/10.1021/ic402186p | Inorg. Chem. 2013, 52, 12818−12827

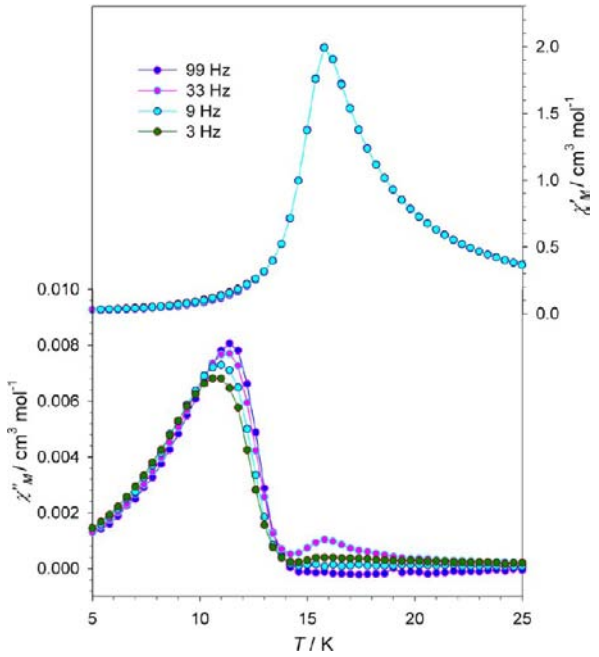

Figure 6. ac-magnetic susceptibility data for **1**. The upper and lower parts depict the in-phase (χ') and out- of-phase (χ'') data, respectively. The ac-susceptibility was measured in an ac field of amplitude 3 G and oscillating frequencies of 3 (green circles), 9 (cyan circles), 33 (pink circles), and 99 Hz (blue circles). The lines are only a guide for the eye.

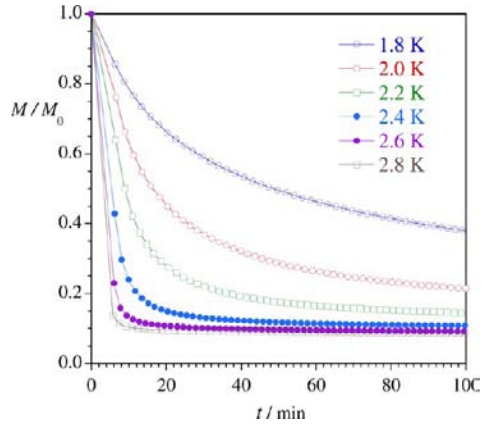

Figure 7. Magnetization relaxation processes of **1** at different temperatures between 1.8 and 2.8 K (see the text for details).

be related to this slow magnetic relaxation of the magnetization.[16] However, the time-dependent magnetization curves of Figure 7 as well as the frequency-dependent ac measurements (Figure 6) do not obey a single exponential law such as the one from Arrhenius. A fit to the Arrhenius law ($\tau = \tau_0 \exp(E^{\#}/kT)$) with the temperature of the maxima of the imaginary ac susceptibility curves yields $\tau_0 = 2.1 \times 10^{-25}$ s and $E^{\#} = 400$ cm^{-1} (Figure S1 in the Supporting Information), values which are meaningless. In fact, the Mydosh parameter ($F = (\Delta T_m/T_m)/\Delta(\log \nu)$, with ν being the frequency, $\nu = 2\pi\tau$) is $F = 0.045$, indicating the occurrence of several energy barriers, as in the case of the spin glasses.[17]

This slow relaxation of the magnetization from the ferromagnetic phase to the antiferromagnetic one has been also observed from neutron studies (see the Discussion below and Figure 11).

NEUTRON STUDIES

Crystal Structure Refinement of 1 at 20 K. The crystal structure of **1** was also refined from neutron powder diffraction data collected at 20 K on the D1A high-resolution powder diffractometer at ILL. The refined model was similar to that observed in the single-crystal X-ray diffraction experiments; however, neutron diffraction allowed us to accurately locate the hydrogen atoms of the fully deprotonated bta ligand.[6]

The refined monoclinic cell parameters measured at 20 K were $a = 6.09927(6)$, $b = 17.44264(15)$, $c = 4.54433(3)$ Å, $\beta = 115.4346(6)°$, and $V = 436.601(7)$ Å^3. Profile R-factors R_p and R_{wp} were 2.8 and 3.4%, respectively. The observed and calculated profiles as well as the difference between them are shown in Figure 8. The X-ray crystal structure collected at 100 K was taken as the initial structural model for the neutron refinements. The atomic coordinates obtained through the neutron diffraction data refinement as well as selected bond lengths and angles are shown in Tables 1 and 2, respectively.

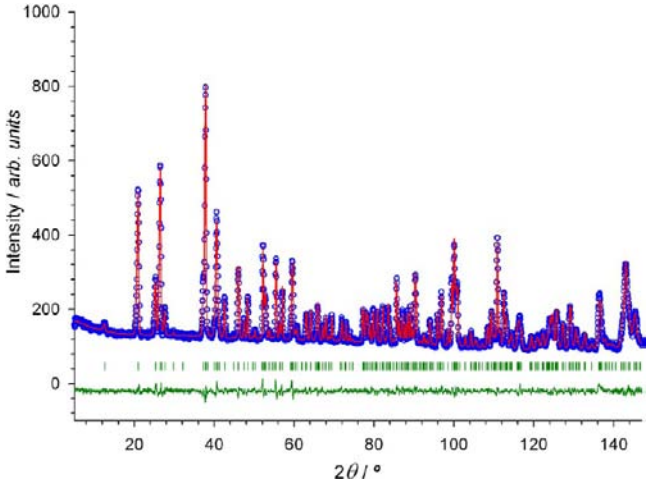

Figure 8. Neutron diffraction pattern of **1** at 20 K: experimental data (blue circles), calculated curve (solid red line), and the difference between them (solid green line). The green vertical lines represent the Bragg positions.

Magnetic Structure of 1. The magnetic structure of **1** was refined by treating the neutron powder diffraction data through the Rietveld method implemented in FullProf.[7] The nuclear structure collected at 20 K on the D1A instrument was taken as the structural model for the later magnetic refinement. The neutron thermodiffractogram (Figure 9) shows a clear increase of intensity on some Bragg reflections below 16 K. This feature is a signature of the appearance of a long-range magnetic order, which is compatible with the magnetic data previously observed by macroscopic magnetometry.[6] It deserves to be noted that the nuclear reflections remain constant in the whole temperature range explored (a lack of extra intensity on top of the nuclear reflections), indicating that the magnetic structure is strictly antiferromagnetic. The magnetic reflections can be indexed using the K-search program included in the FullProf Suite,[18] which involves the six first magnetic reflections that give rise to the propagation vector $\mathbf{k} = (0, 1, 0)$.

To determine the possible magnetic structures compatible with the symmetry of the crystal structure of **1**, we have used the representational analysis techniques described by Bertaut.[19] The propagation vector group $\mathbf{G}_k$ (little group) coincides with the space group $C2/m$ because all rotational symmetry

dx.doi.org/10.1021/ic402186p | Inorg. Chem. 2013, 52, 12818−12827

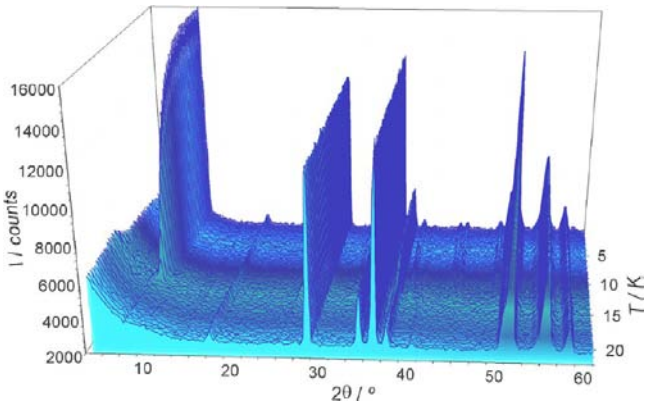

Figure 9. Thermodiffractogram of **1** showing the regularity of the nuclear phase as a function of the temperature and the appearance of magnetic peaks at 16 K.

operators leave **k** invariant. The four irreducible representations (irreps) of the $\mathbf{G}_k$ group were calculated using the BasIreps program (included in the FullProf Suite).[20]

The magnetic representation Γ_M for the magnetic site (Wyckoff position 4h for Co(1)) can be decomposed as a direct sum of irreps by applying the great orthogonality theorem, giving rise to the following decomposition:

$$\Gamma_{4h} = \Gamma_1 \oplus \Gamma_2 \oplus 2\Gamma_3 \oplus 2\Gamma_4$$

In the present case with **k** = (0, 1, 0), all of the irreducible representations are 1D and physically possible. A detailed list of the basis vector for all irreducible representations (Γ_1–Γ_4) is shown in Table 3. The degrees of freedom is 1 (0, u, 0) for the

Table 3. Magnetic Moments of the Contents of a Primitive Cell Deduced for the Four Possible Irreducible Representations (Γ_1–Γ_4) for the Magnetic Site (Co(4h) = (0, 0.2164, 1/2))[a]

	Γ_1 (+ + + +)	Γ_2 (+ + − −)	Γ_3 (+ − + −)	Γ_4 (+ − − +)
m(1)	(0, u, 0)	(0, u, 0)	(u, 0, v)	(u, 0, v)
m(2)	(0, u, 0)	(0, −u, 0)	(u, 0, v)	(−u, 0, −v)

[a]The symmetry operators relating the positions are (1) = *x*, *y*, *z*; and (2) = −*x*, −*y*, −*z*. The characters (sequence of ± signs) of the representations of the *C*2/*m* group with the propagation vector **k** = (0, 1, 0) follow the ordering of the symmetry operations as *E*, 2$_y$, *i*, m_{xz}.

magnetic structure described by Γ_1 and Γ_2, whereas it is 2 (u, 0, v) for Γ_3 and Γ_4. The magnetic moment in any atom position of the crystal can be calculated by means of the Fourier series $\mathbf{m}_l(j) = \sum_{\mathbf{k}} \mathbf{m}_{\mathbf{k}}(j) e^{-2\pi i \mathbf{k} \mathbf{R}_l} = \mathbf{m}_{\mathbf{k}}(j)(-1)^{(2l_2+s)}$, where j indexes the different magnetic atoms in the primitive cell, l labels the unit cell at $\mathbf{R}_l$, which in the case of a centered cell has the form $\mathbf{R}_l = l_1\mathbf{a} + l_2\mathbf{b} + l_3\mathbf{c} + s\mathbf{t}_C$ where l_i are integers, s is 0 or 1, and $\mathbf{t}_C = 1/2\mathbf{a} + 1/2\mathbf{b}$. $\mathbf{m}_{\mathbf{k}}(j)$ is the Fourier component of the magnetic moment of atom j that for a single propagation vector of the form **k** = 1/2**H** (with **H** being a reciprocal lattice vector) is a real vector $\mathbf{m}_{\mathbf{k}}(j) = \mathbf{m}(j)$ that can be identified with the magnetic moment.

The general results extracted from the four possible irreducible representations correspond to antiferromagnetic systems (the propagation vector is in the surface of the Brillouin zone) with a different arrangement of the magnetic moments. The magnetic moments for the Γ_1 and Γ_2 irreducible representations are along the crystallographic *b* axis. Γ_1 has the moment of each cobalt(II) sublattice antiparallel within the *ac* plane, and each plane is magnetically identical, following an *AA* sequence (Scheme 1a). This situation is not compatible with

Scheme 1. Simplified Representation of the Magnetic Structures Obtained from Γ_1– Γ_4 Irreducible Representations

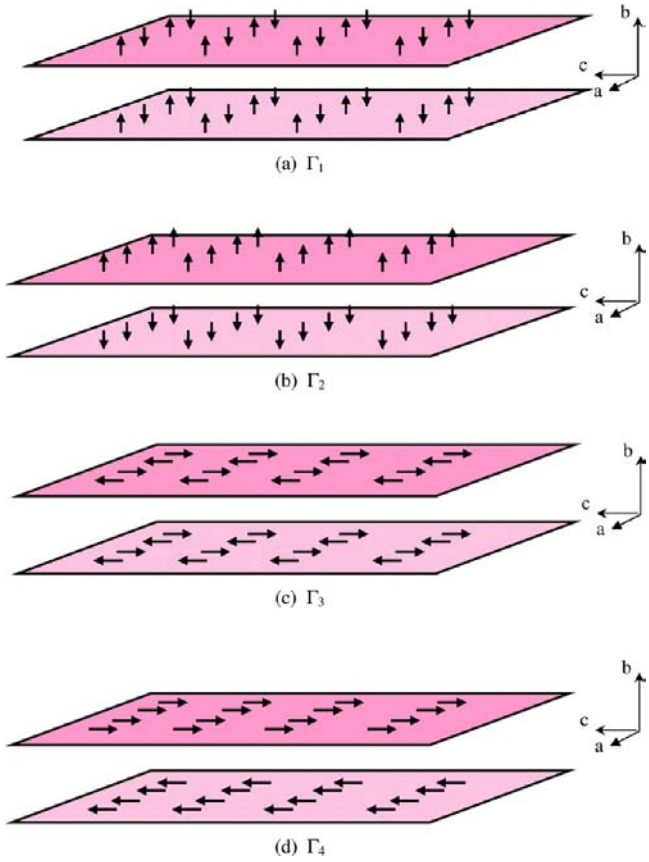

the dominant ferromagnetic interactions observed in the susceptibility measurements for T > 16 K (paramagnetic regime), whereas Γ_2 holds the moments parallel within the *ac* planes but antiferromagnetically coupled with the adjacent planes (Scheme 1b). This model is compatible with the magnetometer measurements, but it is not well-matched with the neutron diffraction patterns. The magnetic moments for the Γ_3 and Γ_4 irreducible representations are contained within the *ac* plane. Γ_3 has the moment of each cobalt(II) ion coupled antiferromagnetically within the *ac* plane, and each *ac* plane is magnetically identical (Scheme 1c). This model (as occurs for Γ_1) is not compatible with the previous susceptibility measurements. For Γ_4, the structure holds the components of the magnetic moments of the cobalt(II) ions parallel within the *ac* plane but coupled antiferromagnetically between adjacent planes (Scheme 1d). This model is compatible with both the magnetometer measurements and the neutron diffraction experiments; moreover, the analysis of the neutron powder diffraction pattern indicates that the Γ_4 model is the only one that fits properly the full profile (see Figure S2 in the Supporting Information).

The results of the analysis of the experimental data below the ordering temperature are reported in Table 4, and a schematic view of the magnetic structure at 2.0 K is shown in Figure 10.

dx.doi.org/10.1021/ic402186p | *Inorg. Chem.* 2013, 52, 12818–12827

Table 4. Magnetic Structure Parameters and Refinement Details for 1 Obtained by Rietveld Refinements

T (K)	M (μB)	M_x (μB)	M_z (μB)	global χ^{2a}	Bragg R-factor^b	mag. R-factor^c
2.0	2.99(14)	3.26(5)	1.90(22)	5.341	5.206	4.048
5.0	2.86(15)	3.13(5)	1.81(25)	6.688	4.827	5.198
10.5	2.63(15)	2.86(6)	1.74(24)	4.893	4.466	4.685
14.5	0.74(27)	0.40(25)	0.82(28)	6.120	4.204	19.57

^{a}Global χ^2 (Bragg contribution). ^{b}Bragg R-factor for the crystalline structure. ^{c}R-factor for the magnetic structure.

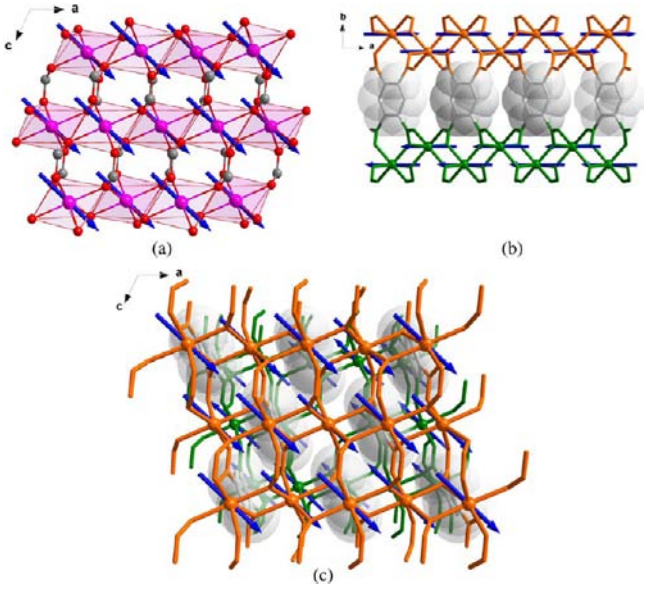

Figure 10. (a) View along the crystallographic b axis of a fragment of the structure of **1**. The skeleton of the bta ligand has been omitted for clarity. (b, c) Detailed view along the crystallographic c (b) and perspective view along the b axes (c) of **1** together with a vector representing the magnetic moment (blue) of the cobalt(II) ions.

These results confirm the existence of a long-range antiferromagnetic ordering. The appearance of a ferromagnetic signal below T_c = 11 K could be due to a weak canting of the antiferromagnetic momenta only in the case where a second propagation vector $\mathbf{k}_2$ = (0, 0, 0) coexists with $\mathbf{k}_1$ = (0, 1, 0) to allow the presence of the ferromagnetic signal needed for the spin-canting explanation. This option was studied through high-flux neutron diffraction patterns collected just above and below the ordering temperature (12 and 2.0 K) during 8 h at each temperature. In principle, the information about the magnetic critical behavior should be accessible by analyzing the temperature dependence of the scattering intensity close to T_N; however, the subtraction of the intensity resulting from the ferromagnetic contribution is rendered difficult because of the weakness of this component. In principle, this experiment should be valid to confirm the appearance of a spin-canting, but it is not enough to discard it if the corresponding component is too small. In any case, the effect of the canting was not detected in our neutron experiments.

Neutron Studies under External Magnetic Field. The slow magnetic relaxation was also studied using neutron diffraction techniques. As shown in Figure 7, the behavior of the slow relaxation curves is temperature-dependent, indicating that the thermal effects play an important role. This relaxation process as a function of the temperature has been measured at 2.0 K using the D1B neutron diffractometer after applying an external field of 2 T (Figure 11). Each diffraction pattern was collected during 5 min, and the relaxation process is clearly appreciable during the first 2 h. After that period, the increase of the intensity of the magnetic peaks is negligible. The full width at half maximum (FWHM) of the magnetic peaks is closely related with the size of the well-ordered antiferromagnetic domains. Assuming that the peak shape is mainly Lorentzian, as the values of the shape parameter suggest, the

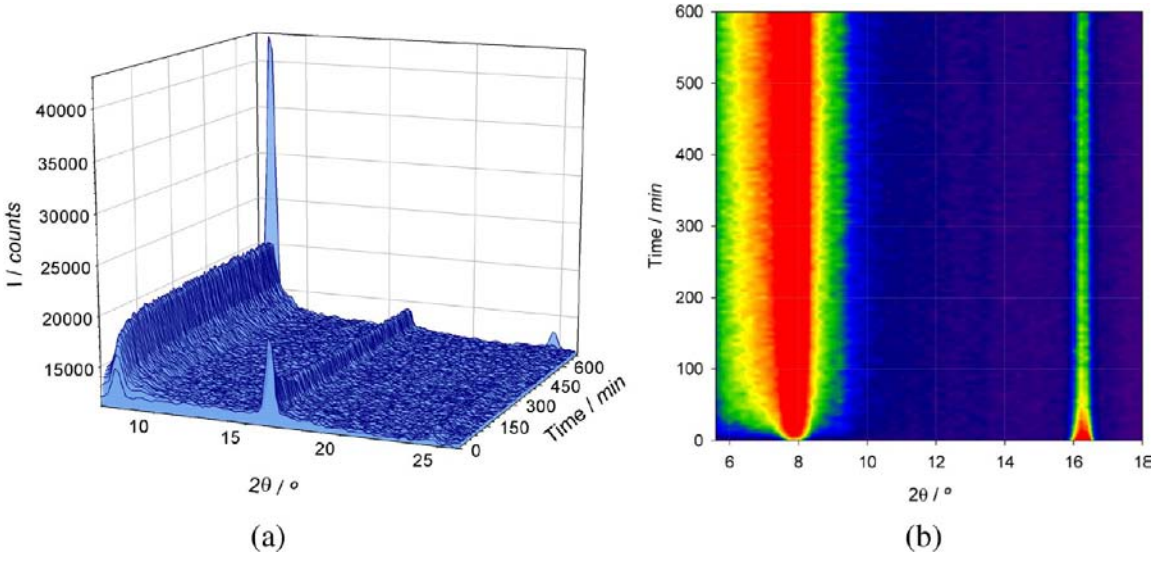

Figure 11. Time-dependence measurement in D1B with the TASMAG cryomagnet collected at 2.0 K: (a) 3D representation and (b) mesh plot. The zero time pattern corresponds to the data collected at H = 2 T. The others were collected at H = 0 T as a function of time. The last pattern in the 3D plot shows the diffraction profile after a ZFC procedure for comparison purposes.

dx.doi.org/10.1021/ic402186p | Inorg. Chem. 2013, 52, 12818−12827

average value of the apparent size was determined for different temperatures (Table 5) using the microstructural option automatically available in FullProf.[7] The increase of the magnetic diffuse scattering after removing the external magnetic field suggests that the structure of the domains has an important nonordered contribution, as was observed by the background increase in the first diffraction patterns collected just after removing the external applied field (Figures 11 and S2 in the Supporting Information).

Table 5. Volume-Averaged Apparent Size (Coherence Length in Å) of the Antiferromagnetic Domains as a Function of the Temperature (K)

2 K	67(4) Å
3 K	93(5) Å
4 K	101(5) Å
5 K	116(5) Å
6 K	135(5) Å
8 K	265(12) Å
11 K	767(69) Å

The neutron measurements under magnetic field show how the system evolves from an antiferromagnet $\mathbf{k} = (0, 1, 0)$ toward a field-induced metamagnet $\mathbf{k}_1 = (0, 1, 0) + \mathbf{k}_2 = (0, 0, 0)$. Three neutron diffraction patterns at 2.0 K are displayed in Figure 12, one corresponding to a ZFC sample (red), another collected under an applied magnetic field of 2 T (blue), and the third one gathered 10 h after removal of the applied magnetic field (green). The comparison between the red and green diffraction patterns shows a small difference in the first nuclear peak (020). This increase of intensity in the green pattern reveals the presence of a remaining weak ferromagnetic contribution from the field-induced metamagnetic phase (inset of Figure 12).

DISCUSSION

The analysis of the magneto-structural data of **1** shows that the μ-oxo(carboxylate) and *anti-syn* carboxylate bridges provide the exchange pathways for the ferromagnetic couplings within the *ac* plane. It is clear that the long-range antiferromagnetic order is reached at 16 K, as supported by the specific-heat curves[6] and the neutron studies performed in this work (Figure 9). The origin of the weak ferromagnetism observed at low temperatures under small applied magnetic fields and of its corresponding out-of-phase signal in the ac-susceptibility measurements are unknown.

There are two explanations that are the most probable. One of them involves a small canting of the Co(II) moments, as suggested by previous authors.[6] In such a situation, the canting angle would be extremely small (ca. 10^{-4} degrees) with a very low effective net magnetic moment (ca. 1.8×10^{-4} BM) (calculated from the χ vs T curve under an applied magnetic field of 1 G).[21] The other one deals with the existence of microdomain structures and/or defects (stacking faults along the crystallographic axis), which can produce a net weak ferromagnetism.

The first option would require the inclusion of a second propagation vector, but no evidence for this has been observed in the zero-field neutron experiments. Moreover, the symmetry analysis of the crystal structure through the Dzyaloshinskii–Moriya[22,23] antisymmetric exchange mechanism,[24] involving the actual space group, precludes the occurrence of a spin-canted structure.[13] Only a nuclear-phase transition without an inversion center occurring at low temperatures (below 20 K) would render the spin canting possible, but this transition has not been observed in the neutron experiments (Figure 9). Furthermore, data collection on the high-intensity neutron diffractometer D1B has been carried out below and above T_c over 8 h to observe the small increase in the nuclear peak resulting from the ferromagnetic order of the spin-canted phase. Nevertheless, no appreciable differences were found. Our alternative explanation to the ferromagnetic signal is based on the introduction of defects in the stacking of the inorganic layers. Therefore, a regular antiferromagnetic alignment of the ferromagnetic layers in the form $(+ - + - + -)$ can be changed in to $(+ - + + - + -)$, producing a net ferromagnetic signal that is contained in the *ac* plane.

Actually, the small increase in the magnetic moment observed in the χ versus T plot, at low temperatures and very low applied magnetic fields, has been considered the main evidence favoring the spin-canting mechanism. This effect disappears when an external magnetic field as low as 100 G is applied. In addition, the magnetic moment of the spin canting is not constant, and it increases with the field (inset of Figure 3b), suggesting that the magnetic moments of the sublattices rotate proportionally to the strength to the applied field. In this sense, the sharp increase of the magnetization below 11 K and $H \approx 1$ G could be explained through the presence of stacking faults in the ferromagnetic layers, producing a net ferromag-

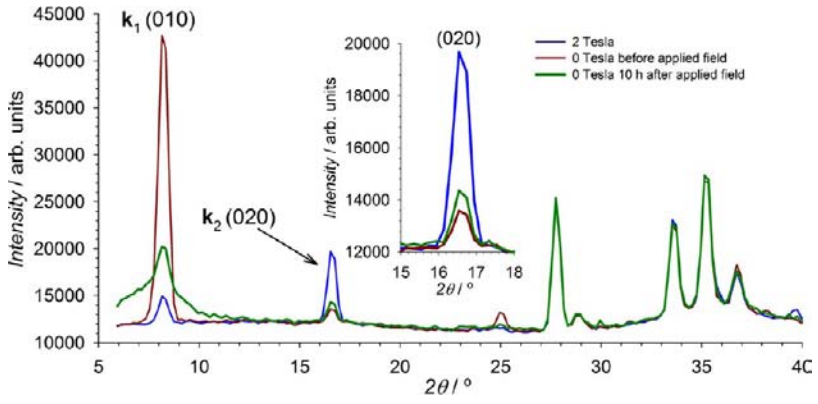

Figure 12. Neutron powder patterns of **1** collected at 2.0 K with the D1B diffractometer using the TASMAG cryomagnet under three different conditions (see the text for details). The inset shows a detailed view of the first nuclear reflection (020).

dx.doi.org/10.1021/ic402186p | Inorg. Chem. 2013, 52, 12818–12827

netic moment within the *ac* plane (Scheme 1). When the magnetic field increases, the energy supplied to the system helps to reduce the number of defects. When $H > 1000$ G, the magnetic moments of the ferromagnetic layers rotate toward the direction of the external applied field. The sigmoidal magnetization curves (Figure 4) and ac-susceptibility measurements as a function of the applied magnetic field (Figure 5) support this hypothesis with a critical field for the metamagnetic transition of 1800 G.

The slow relaxation process in **1** has been studied using the SQUID magnetometer (Figure 7) and neutron diffraction techniques (Figure 11), with both measurements being in total agreement. After the removal of the external applied field, the antiferromagnetic domains start to increase until they are blocked so that traces of a second ferromagnetic phase still coexist. This effect could be explained as a competition between the domain-reorientation energy and the thermal-blocking energy, which produce the slow relaxation process. The mean size (coherence length) of the AF domains as a function of the sample temperature is gathered in Table 3. Other effects are also observed in Figure 11, including the broadening of the magnetic peaks after the application of the external magnetic field together with an increase of the magnetic diffuse scattering. These are evidence of an inhomogeneous network, and the increase of the magnetic diffuse scattering suggests that the structure of domains has an important nonordered contribution. This effect is better observed at lower temperatures where the size of the antiferromagnetic domains is smaller, producing an increase of the proportion between surface domain (nonordered) with respect to the bulk domain (ordered).[25]

Figure 11 shows, in addition to the AF $\mathbf{k}_1 = (0, 1, 0)$ phase, an intrinsic secondary F-phase $\mathbf{k}_2 = (0, 0, 0)$ within the *ac* plane apparent in the form of a slight difference in the first nuclear reflection (020) between the ZFC diffraction pattern and the one collected 10 h after the removal of the external applied field. In principle, the origin of this ferromagnetic phase must be responsible for the high coercive field present in the hysteresis loop observed in the SQUID measurements. Because it is not feasible to carry out the diffraction experiment under magnetic field on a single crystal, we are presently unable to give the volume fraction of this F-phase and the orientation and modulus of the magnetic moments. The only thing that we can say is that this effect diminishes as the temperature increases, a feature that is consistent with the decreasing of the area of the hysteresis loops when the temperature increases.

CONCLUSIONS

The topology of the crystal structure provides the basis for the strong magnetic exchange through the zigzag chain via the μ-oxo(carboxylate) pathway along the crystallographic *a* axis and a secondary exchange route via the *anti-syn* carboxylate bridges. The effects of complementarity/counter-complementarity or anisotropies resulting from the nature of cobalt(II) ions produce a magnetically ordered state with the magnetic moments lying in the *ac* plane, in contrast with those encountered in the divalent transition-metal hydroxides [ß-$Co(OH)_2$ and $Ni(OH)_2$][26] (model b in Scheme 1), for which the moment is perpendicular to the magnetic layers. Nevertheless, when the distance between inorganic layers are increased, like in the molecular-based M(II)-hydroxyl-terephthalate systems [where M(II) = Co(II) or Mn(II)], a similar in-plane magnetic behavior has been previously observed.[27] The reported magnetic structure shows similar magnetic moments arrangement to those observed for model c in Scheme 1. The distance between inorganic layers for these complexes is ca. 9.96 Å, slightly longer that those observed in **1**, ca. 8.79 Å. Although the measurements at the SQUID magnetometer show that **1** behaves as a weak ferromagnet with a T_c of 11 K and as an antiferromagnet with a T_N of 16 K, the neutron diffraction data at zero field only confirms the presence of antiferromagnetic long-range ordering below 16 K, with the magnetic moments ferromagnetically ordered within the layer in the *ac* plane and antiferromagnetically coupled between layers.

The symmetry analysis and the fact of the propagation vector is on the surface of the Brillouin zone evidence that the observed ferromagnetic component cannot be explained in terms of an intrinsic effect, which is the assumption of spin canting. Only the occurrence of a phase transition to a primitive cell or the inclusion of a $\mathbf{k}_2 = (0, 0, 0)$ propagation vector that is not observed in the zero-field measurements may allow for an explanation in terms of spin canting. This possibility could not be completely discarded, but the most plausible solution is based on the presence of stacking faults, which easily produce a net macroscopic ferromagnetic component, as demonstrated by neutron diffraction data taken under applied magnetic field.

Systematic neutron studies of similar compounds, with higher long-range ferromagnetic moments, will be the most useful tool to understand the chemistry and physics of organic–inorganic layered materials.

ASSOCIATED CONTENT

Supporting Information

Structure determination and refinement details, X-ray crystallographic data in CIF format, Arrhenius plot obtained from the ac-susceptibility data, Rietveld refinement of the neutron diffraction pattern (D1B) collected at 2 K, and temperature dependence of the neutron powder patterns after the FC protocol. This material is available free of charge via the Internet at http://pubs.acs.org.

AUTHOR INFORMATION

Corresponding Authors

*E-mail: fabelo@ill.fr (O.F.).
*E-mail: jpasang@ull.edu.es (J.P.).

Notes

The authors declare no competing financial interest.

ACKNOWLEDGMENTS

The authors are grateful to Dr. C. Ritter (Institut Laue Langevin) for access to the D1A diffractometer for the neutron high-resolution measurements. We are grateful to the ILL and Spanish-CRG instruments for the neutron beam time allocated. Partial funding for this work is provided by the Ministerio Español de Ciencia e Innovación through projects MAT2010-16981, CTQ2010-15364, DPI2010-21103-C04-03, MAT2011-27233-C02-02, and MAT2011-25991, by "Factoría de Cristalización" (Consolider-Ingenio2010, CSD2006-00015), and by the Generalitat Valenciana (ISIC/2012/002). J.P. is grateful for the postdoctoral contract (Consolider-Ingenio2010, CSD2006-00015).

REFERENCES

(1) (a) Ouellette, W.; Prosvirin, A. V.; Whitenack, K.; Dunbar, K. R.; Zubieta, J. *Angew. Chem., Int. Ed.* **2009**, *48*, 2140−2143. (b) Ohkoshi, S.; Hamada, Y.; Matsuda, T.; Tsunobuchi, Y.; Tokoro, H. *Chem. Mater.* **2008**, *20*, 3048−3054. (c) Wang, Z. M.; Hu, K. L.; Gao, S.; Kobayashi, H. *Adv. Mater.* **2010**, *22*, 1526−1533. (d) Zhang, W. X.; Xue, W.; Chen, X. M. *Inorg. Chem.* **2011**, *50*, 309−316. (e) Okawa, H.; Sadakiyo, M.; Yamada, T.; Maesato, M.; Ohba, M.; Kitagawa, H. *J. Am. Chem. Soc.* **2013**, *135*, 2256−2262. (f) Tranchemontagne, D. J.; Mendoz-Cortes, J. L.; O'Keeffe, M.; Yaghi, O. M. *Chem. Soc. Rev.* **2009**, *38*, 1257−1283. (g) Horike, S.; Shimomura, S.; Kitagawa, S. *Nat. Chem.* **2009**, *1*, 695−704. (h) Ferey, G. *Chem. Soc. Rev.* **2008**, *37*, 191−214.

(2) (a) Fabelo, O.; Cañadillas-Delgado, L.; Pasán, J.; Delgado, F. S.; Lloret, F.; Cano, J.; Julve, M.; Ruiz-Pérez, C. *Inorg. Chem.* **2009**, *48*, 11342−11351. (b) Cañadillas- Delgado, L.; Fabelo, O.; Cano, J.; Pasán, J.; Delgado, F. S.; Lloret, F.; Julve, M.; Ruiz-Pérez, C. *CrystEngComm* **2009**, *11*, 2131−2142. (c) Cañadillas-Delgado, L.; Pasán, J.; Fabelo, O.; Julve, M.; Lloret, F.; Ruiz-Pérez, C. *Polyhedron* **2013**, *52*, 321−332.

(3) (a) Drillon, M.; Panissod, P. J. *Magn. Magn. Mater.* **1998**, *188*, 93−99. (b) Panissod, P.; Drillon, M. In *Magnetism: Molecules to Materials, IV*; Miller, J. S., Drillon, M., Eds.; Wiley-VCH: Weinheim, Germany, 2002; pp 233−269.

(4) (a) *Neutron Scattering from Magnetic Materials*; Tapan, C., Ed.; Elsevier: Boston, MA, 2006. (b) Izyumov, Y. A.; Naish, V. E.; Ozerov, R. P. *Neutron Diffraction of Magnetic Materials*; Consultants Bureau: New York, 1991.

(5) (a) Cañadillas-Delgado, L.; Fabelo, O.; Rodríguez-Velamazán, J. A.; Lemee-Cailleau, M. H.; Mason, S. A.; Pardo, E.; Lloret, F.; Zhao, J. P.; Bu, X. H.; Simonet, V.; Colin, C. V.; Rodríguez-Carvajal, J. *J. Am. Chem. Soc.* **2012**, *134*, 19772−19781. (b) Baker, M. L.; Mutka, H. *Eur. Phys. J.: Spec. Top.* **2012**, *213*, 53−68. (c) Fabelo, O.; Cañadillas-Delgado, L.; Puente Orench, I.; Rodríguez-Velamazán, J. A.; Campo, J.; Rodríguez-Carvajal, J. *Inorg. Chem.* **2011**, *50*, 7129−7135. (d) Pellaux, R.; Schmalle, H. W.; Huber, R.; Fischer, P.; Hauss, T.; Ouladdiaf, B.; Decurtins, S. *Inorg. Chem.* **1997**, *36*, 2301−2308. (e) Mesbah, A.; Sibille, R.; Mazet, T.; Malaman, B.; Lebegue, S.; Francois, M. *J. Mater. Chem.* **2010**, *20*, 9386−9391.

(6) (a) Snejko, N.; Gutiérrez-Puebla, E.; Martínez, J. L.; Monge, M. A.; Ruiz-Valero, C. *Chem. Mater.* **2002**, *14*, 1879−1883. (b) Kumagai, H.; Kepert, C. J.; Kurmoo, M. *Inorg. Chem.* **2002**, *41*, 3410−3422. (c) Kumagai, H.; Chapman, K. W.; Kepert, C. J.; Kurmoo, M. *Polyhedron* **2003**, *22*, 1921−1927.

(7) Rodríguez-Carvajal, J. *Phys. B* **1993**, *192*, 55−69 The programs of the FullProf Suite and their corresponding documentation can be obtained from the Web at http://www.ill.eu/sites/fullprof/.

(8) The topological analysis was performed using the TOPOS 4.0 program: Blatov, V. A. *IUCr CompComm Newsl.* **2006**, *7*, 4−38.

(9) (a) Fabelo, O.; Pasán, J.; Lloret, F.; Julve, M.; Ruiz-Pérez, C. *CrystEngComm* **2007**, *9*, 815−827. (b) Luo, Y.; Bernot, K.; Calvez, G.; Freslon, S.; Daiguebonne, C.; Guillou, O.; Kerbellec, N.; Roisnel, T. *CrystEngComm* **2013**, *15*, 1882−1896.

(10) (a) Ruiz-Pérez, C.; Rodríguez-Martín, Y.; Hernández-Molina, M.; Delgado, F. S.; Pasán, J.; Sanchíz, J.; Lloret, F.; Julve, M. *Polyhedron* **2003**, *22*, 2111−2123. (b) Rodríguez-Martín, Y.; Hernández-Molina, M.; Delgado, F. S.; Pasán, J.; Ruiz-Pérez, C.; Sanchíz, J.; Lloret, F.; Julve, M. *CrystEngComm.* **2002**, 522−535. (c) García-Terán, J. P.; Castillo, O.; Luque, A.; García-Couceiro, U.; Román, P.; Lloret, F. *Inorg. Chem.* **2004**, *43*, 5761−5770.

(11) Pardo, E.; Faus, J.; Julve, M.; Lloret, F.; Muñoz, M. C.; Cano, J.; Ottenwaelder, X.; Journaux, Y.; Carrasco, R.; Blay, G.; Fernández, I.; Ruiz-García, R. *J. Am. Chem. Soc.* **2003**, *125*, 10770−10771.

(12) (a) Lloret, F.; Ruiz, R.; Julve, M.; Faus, J.; Journaux, Y.; Castro, I.; Verdaguer, M. *Chem. Mater.* **1992**, *4*, 1150−1153. (b) Zurowska, B.; Mrozinski, J.; Julve, M.; Lloret, F.; Maslejova, A.; Sawka-Dobrowolska, W. *Inorg. Chem.* **2002**, *41*, 1771−1777.

(13) Armentano, D.; De Munno, G.; Lloret, F.; Palii, A. V.; Julve, M. *Inorg. Chem.* **2002**, *41*, 2007−2013.

(14) Lloret, F.; Julve, M.; Cano, J.; Ruiz-García, R.; Pardo, E. *Inorg. Chim. Acta* **2008**, *361*, 3912−3918.

(15) Escuer, A.; Cano, J.; Goher, M. A. S.; Journaux, Y.; Lloret, F.; Mautner, F. A.; Vicente, R. *Inorg. Chem.* **2000**, *39*, 4688−4695.

(16) Sibille, R.; Mazet, T.; Malaman, B.; Gaudisson, T.; François, M. *Inorg. Chem.* **2012**, *51*, 2885−2892.

(17) Mydosh, J. A. *Spin Glasses*; Taylor & Francis: Washington, DC, 1993.

(18) Rodríguez-Carvajal, J. *K-Search Program*; Institut Laue−Langevin: Grenoble, France, 2007.

(19) Bertaut, E. F. In *Magnetism*; Rado, G. T., Suhl, H., Eds.; Academic Press: New York, 1963; Chapter 4.

(20) Rodríguez-Carvajal, J. *BasIreps: A Program for Calculating Irreducible Representation of Little Groups and Basis Functions of Polar and Axial Vector Properties*; Institut Laue−Langevin: Grenoble, France, 2010.

(21) Kahn, O. *Molecular Magnetism*; VCH Publishers: New York, 1993.

(22) Dzyaloshinskii, I. E. *J. Exp. Theor. Phys.* **1958**, *6*, 621−622.

(23) (a) Moriya, T. *Phys. Rev.* **1960**, *117*, 635−647. (b) Moriya, T. *Phys. Rev.* **1960**, *120*, 91−98.

(24) Ferrer, S.; Lloret, F.; Pardo, E.; Clemente-Juan, J. M.; Liu-González, M.; García-Granda, S. *Inorg. Chem.* **2012**, *51*, 985−1001.

(25) Becerra, C. C.; Barbeta, V. B.; Paduan-Filho, A.; Palacio, F.; Campo, J.; Gabás, M. *Phys. Rev. B* **1997**, *56*, 3204−3211.

(26) (a) Takada, T.; Bando, Y.; Kiyama, M.; Miyamoto, H.; Sato, T. *J. Phys. Soc. Jpn.* **1966**, *21*, 2726. (b) Takada, T.; Bando, Y.; Kiyama, M.; Miyamoto, H.; Sato, T. *J. Phys. Soc. Jpn.* **1966**, *21*, 2745−2746.

(27) (a) Feyerherm, R.; Loose, A.; Rabu, P.; Drillon, M. *Solid State Sci.* **2003**, *5*, 321−326. (b) Sibille, R.; Mesbah, A.; Mazet, T.; Malaman, B.; Capelli, S.; François, M. J. *Solid State Chem.* **2012**, *186*, 134−141.